Methodology Oriented Thermoelectric Transport Properties of $CaMn_{0.98}Nb_{0.02}O_3$

Rapaka S C Bose, Abanti Nag

Abstract—Perovskite *n*-type $CaMn_{0.98}Nb_{0.02}O_3$ compound is synthesized by three different synthesis methodology: solid-state, sol-gel and combustion synthesis. Phase purity and microstructure of the synthesized samples are investigated by using powder *X*-ray diffraction and scanning electron microscopy, respectively. The electrical resistivity values of all the samples of $CaMn_{0.98}Nb_{0.02}O_3$, synthesized by three different methodology, decrease with increasing temperature as expected from the presence of Mn^{3+} ions with e_g electron in the Mn^{4+} matrix of $CaMnO_3$. The transport properties are explained by Mott's small polaron hopping mechanism. In the high temperature range, $CaMn_{0.98}Nb_{0.02}O_3$ phase synthesized by combustion synthesis exhibits large Seebeck co-efficient (S_{975K} = -162 μVK^{-1}) and low electrical resistivity (ρ_{975K} = 16 mΩ.cm) values, results in a high power factor of 143 $\mu Wm^{-1}K^{-2}$ at 975 K. The above phenomena can be interpreted as variation in porosity of $CaMn_{0.98}Nb_{0.02}O_3$ arising from the different synthesis route where combustion method results in lowest porosity among the other methodologies.

Index Terms— Perovskite oxide, Calcium Manganate, Doping, Density, Methodology, Seebeck Coefficient, Electrical Resistivity,

1 Introduction

Nowadays thermo-electric energy conversion technology turns out to be a potential technology to enable the direct conversion of heat into electrical energy. Generally, the energy conversion efficiency of thermoelectric materials is expressed by the dimensionless figure of merit, $ZT = S^2T/\rho\kappa$, where Z and T are the figure of merit and the absolute temperature, respectively. To achieve a high figure of merit, thermoelectric materials should satisfy the following physical properties: (i) low thermal conductivity (κ), (ii) low electrical resistivity (ρ) and (iii) large Seebeck coefficient (S)[1]. Even though the state-of-the-art thermoelectric alloys show high ZT values, they usually contain metal elements such as lead, tellurium and antimony and not stable at high temperatures in an open atmosphere. The transition metal oxide based semiconductors on the other hand are more suitable for practical applications at high temperatures in air because of their structural and chemical stabilities, oxidation resistance, simple manufacturing process and low cost[2],[3],[4]. The discovery of Na_xCoO_2 single crystal with high ZT is a greatest achievement for oxide materials as potential thermoelectric candidates[5]. Based on the crystal structure the thermoelectric transition metal oxides are classified as four different classes: (i) wide band-gap semiconductor oxides (ZnO, SnO_2 and In_2O_3), (ii) perovskite based oxides ($SrTiO_3$ and $CaMnO_3$), (iii) layered cobalt oxides (Na_xCoO_2, $Ca_3Co_4O_9$ and $Bi_2Sr_2Co_2O_y$) and (iv) layered oxychalcogenides of BiCuSeO type[6].

It is reported that Nb-substituted perovskite manganites based on $CaMnO_3$ show highest ZT value at high temperature[7],[8]. This is a consequence of electron doping in the nominal level at Mn^{4+} sites of $CaMnO_3$ that results drastic decrease of electrical resistivity; keeping relatively high Seebeck co-efficient which are the important parameters to achieve high thermoelectric performance. Therefore, to understand the effect of different synthesis routes on thermoelectric properties, Nb-substituted $CaMnO_3$ is synthesized through three different synthesis methods viz. solid-state reaction, sol-gel and combustion syntheses. In this paper, we report the synthesis and characterization of $CaMn_{0.98}Nb_{0.02}O_3$ and correlate their crystal structure and micro-structural features with the electronic transport properties.

2 Experimental

Polycrystalline perovskite *n*-type phase of $CaMn_{0.98}Nb_{0.02}O_3$ were synthesized by three different synthesis methodologies: (i) solid-state, (ii) sol-gel and (iii) combustion syntheses.

(i) For solid-state reaction method, the stoichiometric amounts of high purity $CaCO_3$ (Alfa Aesar), MnO_2 (Alfa Aesar), and Nb_2O_5 (Alfa Aesar) were thoroughly mixed with ethanol for 3 h, calcined at 1273 K for 2 h and annealed at 1473 K & 1573 K for several hours with intermediate grinding. The annealed powders were pressed into bars and sintered in air at 1598 K for 1 h and slowly cooled to room temperature.

(ii) For the sol-gel method, $Ca(NO_3)_2.4H_2O$ (Alfa Aesar), $Mn(NO_3)_2.4H_2O$ (Alfa Aesar) and $NbCl_5$ (Alfa Aesar) were dissolved in distilled water. Citric acid ($C_8H_8O_7$, Alfa Aesar) was used as complexing agent and added as metal cation/citric acid molar ratio of 1:2 in order to pre-

vent precipitation and $NbCl_5$ hydrolysis. The resulting solution was stirred on a magnetic stirrer at 353 K for 24 h in order to obtain the gel. The gel was dried initially at 423 K for 2 h and further heat treated in air at 1073 K for 4 h with intermediate grinding in order to remove the remaining organics and decompose of the nitrates in the gel. The resultant powders were pressed as described previously and sintered in air at 1473 K for 5h.

(iii) For the combustion method, $Ca(NO_3)_2.4H_2O$ (Alfa Aesar), $Mn(NO_3)_2.4H_2O$ (Alfa Aesar) and $NbCl_5$ (Alfa Aesar) were used as oxidizers and glycine ($C_2H_5NO_2$, Alfa Aesar) as a combustion fuel with molar ratio of the metal nitrates to fuel to be 1:1. The combustion process involved an exothermic reaction between the oxidizers (metal nitrates) and organic fuel (glycine). The stoichiometric proportions of the metal nitrates and glycine were separately dissolved in distilled water to prepare homogeneous solutions. $NbCl_5$ was dissolved in concentrated hydrochloric acid before addition to the above stock solution. The resulting solution was heated slowly to boiling and dehydrated at 353 K that resulted in the formation of highly viscous gel. Subsequently, the gel frothed and swellebulged with evolution of dense fumes. The reaction lasted for 4-5 min and produced fragile foam that instantly crumbled into powder. The synthesized powder was calcined at 1073 K and sintered at 1473 K for several hours in air.

The phase purity of three $CaMn_{0.98}Nb_{0.02}O_3$ powders was examined by powder X-ray diffraction (PXRD) using Bruker D8 Advance X-ray diffractometer (Ni filtered Cu$K\alpha$ radiation). The morphology of the sintered pellets was investigated by field emission scanning electron microscopy (FESEM) using a FEI Quanta 200 F SEM. The cationic composition of randomly selected particles was analyzed by energy dispersive X-ray spectroscopy (EDX) coupled to SEM. The relative bulk density was measured by the Archimedes method. The electrical resistivity (ρ) and Seebeck coefficient (S) measurements were carried out on a bar-shaped sample ($2 \times 2 \times 13$ mm^3) between 300 and 975 K at ambient pressure using in-house built resistivity and thermopower unit.

3 Results and Discussion

Figure 1(a-c) shows the XRD patterns of $CaMn_{0.98}Nb_{0.02}O_3$ composition, indicating the single-phase nature of the synthesized compounds. The lattice parameters are calculated from XRD patterns and summarized at Table 1. Nb-substitution at the Mn-site of $CaMnO_3$ causes an increase of lattice parameters and cell volume. This can be interpreted by the larger ionic radii of both $Nb^{5+}{}_{VI}$ (0.640 Å) and $Mn^{3+}{}_{VI}$ (0.645 Å), generated in the $Mn^{4+}{}_{VI}$ (0.530 Å) matrix [9]. Further, the calculated density values are listed in Table 1. The highest density is obtained from combustion compound, i.e. 4.12 g/cm^3 (~90%). It is relevant to note that high bulk density is needed to improve the thermoelectric properties.

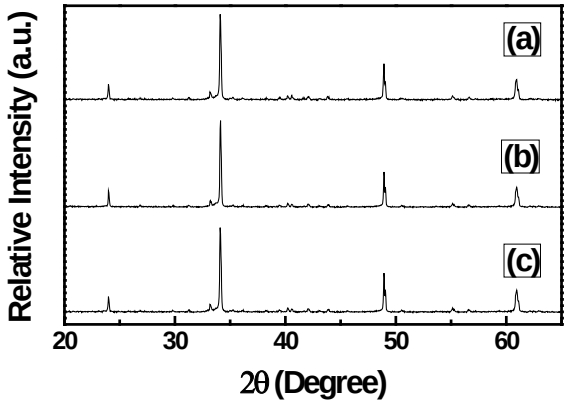

Fig. 1. Powder XRD of (a) Combustion, (b) Sol-gel, (c) Solid-state samples

TABLE 1
Crystallographic and Transport Properties Data

$CaMn_{0.98}Nb_{0.02}O_3$	Solid-state	Sol-gel	Combustion
a (Å)	5.2957	5.2901	5.2823
b (Å)	7.4693	7.4693	7.4537
c (Å)	5.2784	5.2762	5.2706
$b/\sqrt{2}$	5.2816	5.2816	5.2706
V (Å^3)	208.7880	208.4804	207.7303
d (g/cc)	2.74	3.42	4.12
Relative density (%)	61	75	90
ρ_{975K} (mΩ.cm)	43	27	16
S_{975K} (μW K^{-1})	-188	-174	-165
PF_{975K} (μW m^{-1} K^{-2})	82	104	147

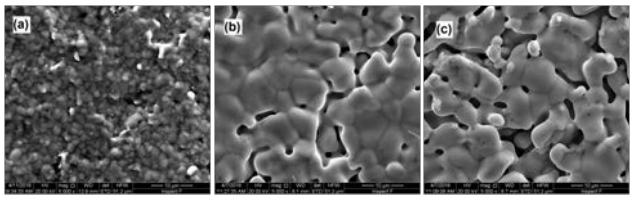

Fig. 2. FESEM micrographs showing cross sections of as sintered pellets of (a) solid-state, (b) Sol-gel, (c) Combustion samples.

Figure 2(a-c) shows field emission scanning electron micrographs of as-sintered cross-section of $CaMn_{0.98}Nb_{0.02}O_3$ developed through different methodology. It is observed from the micrographs that morphological changes occurred due to the synthesis of Nb-substituted $CaMnO_3$ by different routes. The grains are irregularly shaped with rounded corners and smooth grain interfaces irrespective of the synthesis methods. Grains of 4-9 μm, 3-6 μm, and 0.7-2.5 μm are achieved for solid-state, sol-gel and combustion methodologies, respectively. The FESEM images of the sol-gel and combustion compounds suggest that the grains are particularly interconnected leading to the large specific surface area compared to the solid-state compounds, where the FESEM image indicates high porosity. This result is in good agreement with the density measurement. Therefore, micro-structural features have much contribution governing the electronic transport properties of $CaMn_{0.98}Nb_{0.02}O_3$. The cationic compositions of the sol-gel and combustion compounds are in good agreement with the intended compositions, except for the solid-state phase, where the EDX results suggest a lower Nb content than expected. Therefore, it represents more number of Mn^{3+} in sol-gel and combustion synthesized $CaMn_{0.98}Nb_{0.02}O_3$ compared to solid-state synthesized one. It is well known that, in solution-state synthesis processes, i.e. sol-gel and combustion methods, the cations of the perovskite phase are mixed in liquid solution, while in conventional solid-state synthesis, the inter-diffusion of the cations in solid matrix is necessary to homogenize the product phases. Thus, small concentrations of Nb can be fast and homogeneously distributed in the aqueous solutions.

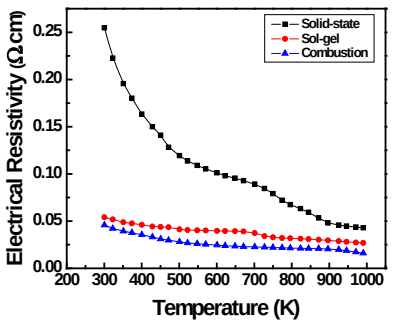

Fig. 3. Temperature dependence of electrical resistivity of $CaMn_{0.98}Nb_{0.02}O_3$.

The temperature dependence of electrical resistivity (ρ) of $CaMn_{0.98}Nb_{0.02}O_3$ is shown in Figure 3. It is repoted that the un-doped $CaMnO_3$ also represents typical semiconductor like behaviour ($d\rho/dT < 0$) with resistivity as high as 2×10^4 mΩ.cm at room temperature[10]. $CaMn_{0.98}Nb_{0.02}O_3$ also show semiconductor like transport behaviour in the temperature range of 300 to 975 K irrespective of the synthetic routes. The substitution by Nb^{5+} at Mn^{4+}-site significantly reduces ρ by several orders of magnitude. The remarkable reduction of electrical resistivity is due to the formation of Mn^{3+} ($t_{2g}^3e_g^1$) ions with e_g^1 electron in the Mn^{4+} ($t_{2g}^3e_g^0$) matrix of Nb-substituted $CaMnO_3$. The electron hopping between Mn^{3+} and Mn^{4+} ions is responsible for the electrical conductivity in perovskite manganites. According to valence equilibrium, the formation of an appreciable concentration of Mn^{3+} introduces free electrons in the e_g orbital which act as a charge carrier in Mn^{3+}–O–Mn^{4+} framework. The electron hopping through double-exchange interaction in Mn^{3+}–O–Mn^{4+} framework causes reduction of ρ. This result is in agreement with structural analyses. It is observed that the resistivity values of solid-state compound are high as compared to the sol-gel and combustion. This can be explained by both porosity and lower Nb-concentration of the sample synthesized through solid-state compound. This in turn results in lower number of Mn^{3+} in the Mn^{4+} matrix leading to high resistivity values for solid-state synthesized sample. And also porosity shows negative impact on the resistivity values i.e. resistivity increases with increasing porosity. Due to the high porosity in the compound, the grains are not interconnected each other. Therefore, the pores act as barriers in the hopping mechanism of charge carriers thereby leading to contribute high resistivity values. For the Nb-substituted $CaMnO_3$ composition, lowest resistivity observed for combustion compound with resistivity value of ρ_{RT} = 45 mΩ.cm and ρ_{975K} = 16 mΩ.cm. Further, both sol-gel and combustion compositions show resistivity nearly same order of magnitude (Fig. 3), indicating presence of equal number electron carriers. The small difference in the resistivity in the order of few milliohms for these two different synthesis routes, sol-gel and combustion syntheses, arises from micro-structural features. The sol-gel compound shows little high electrical resistivity values than combustion compound even if both the compounds synthesized through solution-state. The different morphologies and the size of grains obtained by the two synthesis methods can be considered to explain this. The combustion phase reveals a three times smaller grain size than the sol-gel compounds and a specific area at least twice as high as the sol-gel compounds. Therefore, the contact surface between different grains is larger in the case of the combustion compounds compared to sol-gel compounds. The combustion phases present a particular morphology with good interconnections between the grains, promoting the transport of charge carriers. And also little impact of porosity is present in sol-gel compound since lower density of sol-gel compound than combustion compound. Therefore, it can be concluded that the micro-structural changes have a close correlation with the electrical transport in perovskite manganites. The electrical resstivity values are listed in Table 1.

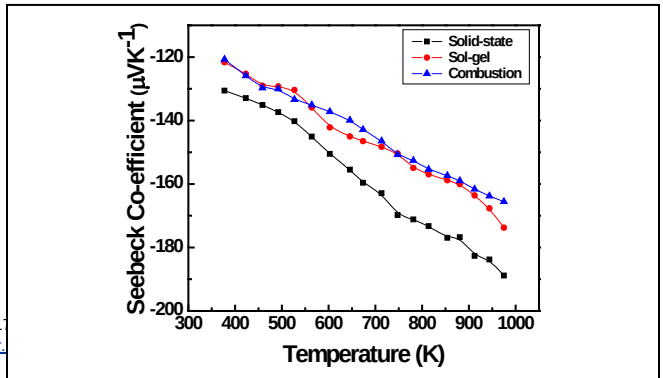

Fig. 4. Temperature dependence of Seebeck coefficient of $CaMn_{0.98}Nb_{0.02}O_3$.

The temperature dependence of Seebeck co-efficient (S) of $CaMn_{0.98}Nb_{0.02}O_3$ is shown in Figure 4. The negative S value in the whole measured temperature range indicates that the dominant charge carriers are electron. Parent $CaMnO_3$ exhibits a large Seebeck co-efficient (S) of about -500 to -600 μV K^{-1} due to its low carrier concentration. The substitution at tetravalent Mn^{4+} sites by pentavalent Nb^{5+}, causes drastic reduction of S values compared to the un-doped $CaMnO_3$. This is in agreement with decrease of ρ and the increase of electron concentration i.e. Mn^{3+} with e_g^1 electron. Identical Seebeck co-efficient values and $S(T)$ behaviour are measured for the compounds since equivalent Nb content irrespective of the synthesis method. This confirms that the different micro-structures of the all three compounds do not influence either the charge carrier concentration or the electronic band structure. The sole exception is the solid-state compound having a slightly higher Seebeck co-efficient values compared to the corresponding sol-gel and combustion compounds. The analysis of the cationic composition reveals a small Nb deficiency for the solid-state compound in comparison to the expected composition, suggesting a higher Mn^{4+} concentration associated with a large S value. The absolute S value at 975 K, S_{975K} = -162 μV K^{-1} is observed for combustion compound. The absolute Seebeck co-efficient values are listed in Table 1.

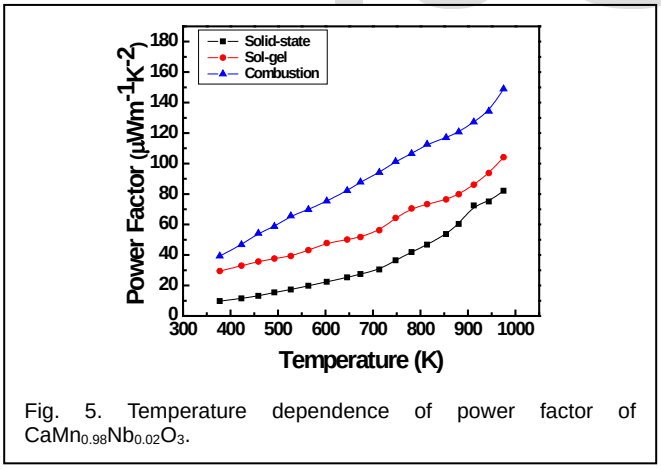

Fig. 5. Temperature dependence of power factor of $CaMn_{0.98}Nb_{0.02}O_3$.

The power factor (S^2/ρ) is calculated from the measured electrical resistivity and Seebeck coefficient of $CaMn_{0.98}Nb_{0.02}O_3$ and plotted as a function of temperature in Figure 5. The undoped $CaMnO_3$ shows the power factor of 12 μW $m^{-1}K^{-2}$ arising from high resistivity (2×10^4 mΩ.cm) and high Seebeck co-efficient (-500 μV $m^{-1}K^{-1}$). It is observed that the power factor for all three Nb-substituted $CaMnO_3$ increase monotonically with temperature. The larger power factor is obtained for combustion $CaMn_{0.98}Nb_{0.02}O_3$ sample due to their relatively lower resistivity of 16 mΩ.cm and moderate Seebeck coefficient of -162 μV $m^{-1}K^{-1}$. The highest power factor of 143 μW $m^{-1}K^{-2}$ is obtained for combustion $CaMn_{0.98}Nb_{0.02}O_3$ sample at 975 K. The power factor obtained for Nb-substituted $CaMnO_3$ is ten times of magnitude higher than that of un-doped $CaMnO_3$.

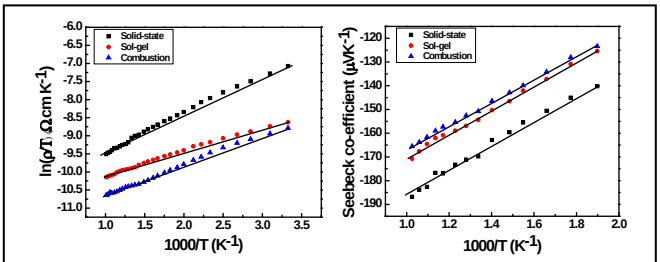

Fig. 6. The linear curve fitting for $ln(1/\rho)$ and S versus $1000/T$ plots for $CaMn_{0.98}Nb_{0.02}O_3$.

To understand the transport mechanism of Nb-substituted $CaMnO_3$, the $\rho(T)$ curves and $S(T)$ curves are fitted according to Mott's adiabatic small polaron conduction model. In this framework, $\rho(T)$ and $S(T)$ can be expressed as [10],[11]

$$\frac{\rho}{T} = \rho_0 \left(exp\frac{E_a}{k_B T}\right)$$

$$S = \frac{k_B}{e}\left(\frac{E_S}{k_B T} + \alpha\right)$$

where, E_a is the activation energy for electrical conduction, E_s is thermopower activation energy required to produce charge carriers, T is the absolute temperature, ρ_0 and α are the constants. Therefore, Mott's small polaron hopping model predicts a linear fit in $\ln(\rho/T)$ vs $1/T$ and $S(T)$ vs $1/T$ plots at high temperature ($T > \theta_D/2$; where θ_D is the Debye temperature). The experimental value of Debye temperature for the manganese-based perovskite oxides are reported to around 400 K[12],[13][14]. Figure 6 shows the linear curve fitting of $ln(\rho/T)$ vs $1/T$ plot for Nb-substituted $CaMnO_3$ above 400 K. Thus, the transport mechanism of Nb-substituted $CaMnO_3$ in the high temperature range ($T > 200$ K) can be interpreted by the small polaron hopping conduction theory of Mott.

4 Conclusion

In conclusion, we report the crystal structure and high temperature transport properties of Nb-substituted $CaMnO_3$ prepared by three different synthesis methods. The enhancement of cell volume supports the formation of Mn^{3+} in the Mn^{4+} matrix. The differences in microstructures influence the transport properties. Combustion sample reveals lower intrinsic electrical resistivity than the solid-state and sol-gel samples, probably due to the better surface contact between the gains and high bulk density. All the three samples yield to equal Seebeck co-efficient values for the $CaMn_{0.98}Nb_{0.02}O_3$ since thermopower

depends on electronic band structure and charge carrier concentrations. The results leads to high power factor value for the combustion sample, that is, PF_{975K} = 143 μW m^{-1} K^{-2}. The transport mechanism of Nb-substituted $CaMnO_3$ in the high temperature range (T > 200 K) can be interpreted by the small polaron hopping conduction theory of Mott.

ACKNOWLEDGMENT

The authors wish to thank Dr. Ramesh Gardas, Associate Professor, Indian Institute of Technology Madras for powder XRD data and FESEM micrographs. This work was supported in part by a grant from Council of Scientific and Industrial Research and Science and Engineering Research Board, Department of Science and Technology, Government of India.

REFERENCES

[1] D. M. Rowe, *Thermoelectrics Handbook: Micro to Nano, CRC Press,* Taylor & Francis Group, USA (2006).

[2] J. W. Fergus, "Oxide materials for high temperature thermoelectric energy conversion," *J. European Ceram. Soc.*, 2012, 32, 525-540.

[3] K. Koumoto, Y.F. Wang, R. Zhang, A. Kosuga, R. Funahashi, "Oxide thermoelectric materials: A nanostructuring approach," *Annu. Rev. Mater. Res.*, 2010, 40, 363-394.

[4] N. N. Van, N. Pryds, "Nanostructured oxide materials and modules for high-temperature power generation from waste heat," *Adv. Nat. Sci.: Nanosci. Nanotechnol.*, 2013, 4, 023002.

[5] I. Terasaki, Y. Sasago, K. Uchinokura, "Large thermoelectric power in $NaCo_2O_4$ single crystals," *Phys. Rev. B* 56, R12685 (1997).

[6] A. Nag, V. Shubha, "Oxide thermoelectric materials: A structure-property relationship," *J. Electron. Mater.*, 2014, **43**, 962-977.

[7] L. Bocher, M. H. Aguirre, D. Logvinovich, A. Shkabko, R. Robert, M. Trottmann, A. Weidenkaff, "$CaMn_{1-x}Nb_xO_3$ ($x \leq 0.08$) perovskite-type phases as promising new high-temperature *n*-type thermoelectric materials," *Inorg. Chem.*, 2008, **47**, 8077-8085.

[8] S. Populoh, M. Trottmann, M. H. Aguire, A. Weidenkaff, "Nanostructured Nb-substituted $CaMnO_3$ n-type thermoelectric material prepared in a continuous process by ultrasonic spray combustion," *J. Mater. Res.*, 2011, **26**, 1947-1952.

[9] R. D. Shannon, "Revised effective ionic radii and systematic studies of interatomic distances in halides and chalcogenides," *Acta Cryst.*, 1976, A32, 751-767.

[10] P. M. Chaikin, G. Beni, "Thermopower in the correlated hopping regime," *Phys. Rev. B*, 1976, **13**, 647.

[11] N. F. Mott, E. A. Davis, in "Electronic Processes in Noncrystalline Materials", Clarendon, Oxford, 1971.

[12] J. J. Hamilton, E. L. Keatley, H. L. Ju, A. K. Raychaudhuri, V. N. Smolyaninova, R. L. Greene, "Low-temperature specific heat of $La_{0.67}Ba_{0.33}MnO_3$ and $La_{0.8}Ca_{0.2}MnO_3$," *Phys. Rev. B*, 1996, **54**, 14926.

[13] M. R. Lees, O. A. Petrenko, G. Balakrishnan, D. McK. Paul, "Specific heat of $Pr_{0.6}(Ca_{1-x}Sr_x)_{0.4}MnO3_{(}0<\sim x<\sim 1)$," *Phys. Rev. B*, 1999, **59**, 1298.

[14] S. Mollah, G. Anjum, H. D. Yang, "Non-adiabatic polaron hopping conduction in $CaMn_{1-x}Cr_xO_3$ ($0 \leqslant x \leqslant 0.3$)," *J. Phys. Chem. Solids*, 2009, **70**, 489-494.